Herschel-ATLAS: the link between accretion luminosity and star formation in quasar host galaxies[⋆]

D. G. Bonfield,[1]† M. J. Jarvis,[1] M. J. Hardcastle,[1] A. Cooray,[2] E. Hatziminaoglou,[3]
R. J. Ivison,[4,5] M. J. Page,[6] J. A. Stevens,[1] G. de Zotti,[7,8] R. Auld,[9] M. Baes,[10]
S. Buttiglione,[7] A. Cava,[11] A. Dariush,[9,12] J. S. Dunlop,[5] L. Dunne,[13] S. Dye,[9]
S. Eales,[9] J. Fritz,[10] R. Hopwood,[14] E. Ibar,[4] S. J. Maddox,[13] M. J. Michałowski,[5]
E. Pascale,[9] M. Pohlen,[9] E. E. Rigby,[13] G. Rodighiero,[7] S. Serjeant,[14] D. J. B. Smith,[13]
P. Temi[15] and P. van der Werf[5,16]

[1]*Centre for Astrophysics Research, Science and Technology Research Institute, University of Hertfordshire, Hatfield AL10 9AB*
[2]*Department of Physics and Astronomy, University of California, Irvine, CA 92697, USA*
[3]*ESO, Karl-Schwarzschild-Str. 2, 85748 Garching bei München, Germany*
[4]*UK Astronomy Technology Centre, Royal Observatory, Edinburgh EH9 3HJ*
[5]*Scottish Universities Physics Alliance, Institute for Astronomy, University of Edinburgh, Royal Observatory, Edinburgh EH9 3HJ*
[6]*Mullard Space Science Laboratory, University College London, Holmbury St. Mary, Dorking, Surrey RH5 6NT*
[7]*INAF – Osservatorio Astronomico di Padova, Vicolo Osservatorio 5, I-35122 Padova, Italy*
[8]*SISSA, Via Bonomea 265, I-34136 Trieste, Italy*
[9]*School of Physics and Astronomy, Cardiff University, Queen's Buildings, The Parade, Cardiff CF24 3AA*
[10]*Sterrenkundig Observatorium, Universiteit Gent, Krijgslaan 281 S9, B-9000 Gent, Belgium*
[11]*Departamento de Astrofísica, Facultad de CC. Físicas, Universidad Complutense de Madrid, E-28040 Madrid, Spain*
[12]*School of Astronomy, Institute for Research in Fundamental Sciences (IPM), PO Box 19395-5746 Tehran, Iran*
[13]*Centre for Astronomy and Particle Theory, The School of Physics and Astronomy, Nottingham University, University Park Campus, Nottingham NG7 1HR*
[14]*Department of Physics and Astronomy, The Open University, Walton Hall, Milton Keynes MK7 6AA*
[15]*Astrophysics Branch, NASA/Ames Research Center, MS 245-6, Moffett Field, CA 94035, USA*
[16]*Leiden Observatory, Leiden University, PO Box 9513, NL-2300 RA Leiden, the Netherlands*

ABSTRACT

We use the science demonstration field data of the *Herschel* Astrophysical Terahertz Large Area Survey to study how star formation, traced by the far-infrared *Herschel* data, is related to both the accretion luminosity and redshift of quasars selected from the Sloan Digital Sky Survey (SDSS) and the 2dF-SDSS luminous red galaxy (LRG) and Quasar Spectroscopic Catalogue survey. By developing a maximum-likelihood estimator to investigate the presence of correlations between the far-infrared and optical luminosities, we find evidence that the star formation in quasar hosts is correlated with both redshift and quasar accretion luminosity. Assuming a relationship of the form $L_{IR} \propto L_{QSO}^{\theta}(1 + z)^{\zeta}$, we find $\theta = 0.22 \pm 0.08$ and $\zeta = 1.6 \pm 0.4$, although there is substantial additional uncertainty in ζ of the order of ± 1, due to uncertainties in the host galaxy dust temperature. We find evidence for a large intrinsic dispersion in the redshift dependence, but no evidence for intrinsic dispersion in the correlation between L_{QSO} and L_{IR}, suggesting that the latter may be due to a direct physical connection between star formation and black hole accretion. This is consistent with the idea that both the quasar activity and star formation are dependent on the same reservoir of cold gas, so that they are both affected by the influx of cold gas during mergers or heating of gas via feedback processes.

Key words: galaxies: active – galaxies: high-redshift – quasars: general.

1 INTRODUCTION

Active galactic nucleus (AGN) activity is now widely believed to be an important phase in the evolution of every massive galaxy

in the Universe. This belief stems firstly from the discovery of a relatively tight correlation between the mass of a galaxy's bulge and the mass of its central supermassive black hole (SMBH; e.g. Magorrian et al. 1998; Ferrarese & Merritt 2000; Gebhardt et al. 2000), which implies that build-up of the stellar mass and the SMBH mass are causally connected (although see also Jahnke & Macciò 2011, who show that averaging of parameters by mergers can also produce such a correlation).

From a more theoretical perspective, AGN have become a key ingredient for semi-analytic models of galaxy formation (e.g. Guiderdoni et al. 1998; Cole et al. 2000; Granato et al. 2001; Benson et al. 2003). The overproduction of stars at the bright end of the galaxy luminosity function by these models has led to the inclusion of an extra source of heating or 'AGN feedback' (see e.g. Granato et al. 2004; Bower et al. 2006; Croton et al. 2006). However, it is still unclear what kind of AGN-driven feedback is the most important, e.g. two complementary mechanisms are described by Croton et al. (2006): 'quasar-mode' feedback, proposed to be effective during episodes of efficient accretion of cold gas, and 'radio-mode' feedback, caused by the relatively inefficient accretion of hot gas (in the absence of cold gas) when an AGN would have lower optical luminosity, but would also be generating radio jets. Thus, it is now clear that if we are to understand galaxy formation and evolution, we must also obtain a clear picture of AGN, their environments and the coevolution of SMBHs and their host galaxies.

It is difficult to study the host galaxies of distant quasars, due to the nuclear quasar emission overwhelming the stellar emission at optical and near-infrared wavelengths. However, *Hubble Space Telescope* and high spatial resolution ground-based imaging have enabled the investigation of the stellar populations of quasar hosts (e.g. Bahcall, Kirhakos & Schneider 1994; McLure et al. 1999; Dunlop et al. 2003; Kotilainen et al. 2009), demonstrating that most luminous quasars reside in massive elliptical galaxies. A number of studies have attempted to determine the star formation properties of quasar host galaxies, with some using optical colours (e.g. Sánchez et al. 2004) or spectroscopy (e.g. Nolan et al. 2001; Silverman et al. 2009; Trichas et al. 2010). Some information on the host galaxies of AGN has been gleaned from powerful radio galaxies, where the quasar nucleus is obscured due to the putative dusty torus (e.g. Antonucci 1993). Again these studies show that powerful AGN reside in massive galaxies (e.g. Jarvis et al. 2001; McLure et al. 2004; Seymour et al. 2007) and there appears to be a trend where the most powerful exhibit signs of recent star formation (e.g. Baldi & Capetti 2008; Herbert et al. 2010). However, optical colours and emission lines can be contaminated by the quasar, so that its contribution must be modelled to estimate the star formation rate (SFR), and all of these studies suffer from the uncertainty arising from having very little information about how much star formation is obscured by dust, and thus how much of the emission due to young stars is reprocessed to far-infrared and submillimetre (submm) wavelengths.

Spectroscopy with the *Spitzer Space Telescope* has enabled the determination of SFRs in individual AGN via mid-infrared emission lines, which are much less susceptible to dust (e.g. Schweitzer et al. 2006; Netzer et al. 2007; Lutz et al. 2008; Martínez-Sansigre et al. 2008; Shi et al. 2009; Trichas et al. 2009; Lutz et al. 2010). However, the relatively low sensitivity of *Spitzer* infrared spectrograph has meant that only small, severely flux-limited samples of objects could be investigated, making the precise relationship between SFR and quasar luminosity difficult to robustly determine.

(Sub)millimetre instruments such as Submillimetre Common-User Bolometer Array (SCUBA) and Max-Planck Millimetre Bolometer Array (MAMBO) have provided important information on reprocessed emission from star formation in distant quasars and radio galaxies, e.g. photometric surveys revealing luminous ($\sim 10^{13}$ L$_\odot$) far-infrared emission from a number of radio galaxies and quasar hosts, making it clear that major (SFR ~ 1000 M$_\odot$ yr^{-1}) episodes of star formation can coexist with powerful AGN (e.g. Archibald et al. 2001; Omont et al. 2003; Priddey et al. 2003; Page et al. 2004; Martínez-Sansigre et al. 2009). Furthermore, submm imaging has revealed overdensities of sources in the vicinity of individual high-z AGN, plausibly belonging to the same large-scale structures (Stevens et al. 2003; Priddey et al. 2007; Stevens et al. 2010). Conversely, cross-correlating SCUBA data with deep X-ray surveys, Alexander et al. (2005) also show that a large fraction of submm galaxies contain buried AGN, while Laird et al. (2010) find that the X-ray AGN fraction in submm galaxies is 20–29 per cent.

The main drawback of the submm studies to date is that, due to the high background associated with ground-based observing and the small number of pixels in existing instruments, it has not been possible to obtain very large samples of objects. A recent study by Serjeant & Hatziminaoglou (2009, hereafter SH09) attempted to overcome this shortfall by combining data from a wealth of *Spitzer* and *Infrared Space Observatory (ISO)* observations at mid- and far-infrared wavelengths to investigate how obscured star formation in the hosts of quasars evolved over cosmic time and also how this may be related to the bolometric output of the AGN. They found evidence for an increase in far-infrared luminosity as a function of both cosmic epoch and quasar luminosity. However, they measured the correlation between far-infrared and quasar luminosity using wide redshift bins, which can potentially confuse the effect of redshift with that of quasar luminosity, since the latter evolves strongly with redshift in flux-density-limited samples. In addition, their work extrapolated the far-infrared flux from mid-infrared wavelengths using spectral energy distribution (SED) templates, and it would clearly be preferable to measure the far-infrared flux directly.

The recently launched European Space Agency (ESA) *Herschel Space Observatory* (Pilbratt 2010) offers an unprecedented combination of sensitive detectors, large (3.5-m diameter) collecting area and low background, which makes it possible, for the first time, to conduct deep surveys of large areas of the sky at far-infrared/submm wavelengths.

In this paper we present a study of the far-infrared fluxes of known quasars in science demonstration (SD) observations of the *Herschel* Astrophysical Terahertz Large Area Survey (H-ATLAS; Eales et al. 2010). This is the first single sample of quasars measured in the submm which is large and diverse enough to directly determine a relationship between far-infrared (cool dust) luminosity and optical (quasar) luminosity, without using infrared information at wavelengths short enough to be possibly contaminated by warm dust in the AGN torus. While Serjeant et al. (2010) determine a relationship between optical and far-infrared luminosity using these data in combination with infrared luminosities derived from shorter wavelength *Spitzer* and *ISO* data, here we use only the H-ATLAS data.

Section 2 describes the H-ATLAS observations used. Section 3 explains how we construct our quasar sample, determine far-infrared fluxes for them and find a maximum-likelihood fit to the relationship between far-infrared luminosity, optical luminosity and redshift. The results of this fitting are discussed in Section 4 and conclusions are presented in Section 5.

2 OBSERVATIONS

When completed, H-ATLAS will provide photometry for 550 deg² of the sky in five far-infrared/submm bands. The 5σ depths at wavelengths of 100, 160, 250, 350 and 500 μm are 132, 126, 32, 36 and 45 mJy, respectively.

In this paper, we use data only from *Herschel*'s Spectral and Photometric Imaging Receiver (SPIRE) instrument (Griffin et al. 2010), at 250, 350 and 500 μm, since the Photodetector Array Camera and Spectrometer (PACS) 100 and 160 μm data (Poglitsch et al. 2010) are not deep enough to provide useful constraints on the infrared luminosities of the quasars we are studying (Ibar et al. 2010). The longer SPIRE wavelengths are also less likely to be contaminated by direct emission from the warm dust of the AGN torus. This means that the emission can be more reliably attributed to cool dust heated by star formation processes, and its SED approximated by a simple greybody.

This paper is also restricted in area to the H-ATLAS SD field, which covers approximately 16 deg² – around 3 per cent of the total survey area. These SD data have been publicly released, and both the maps and catalogues can be retrieved from the H-ATLAS web page.[1]

3 METHOD

Our quasar sample consists of all objects in the field which are identified as quasars in the seventh data release of the Sloan Digital Sky Survey (SDSS) Quasar Catalog (Schneider et al. 2010) or the 2dF-SDSS luminous red galaxy (LRG) and Quasar Spectroscopic Catalogue (2SLAQ; Croom et al. 2009). After removing the known blazar HB0906+015, since its far-infrared emission will not be dominated by star formation (see e.g. González-Nuevo et al. 2010), we find 372 quasars in the whole Science Verification (SV) field, with a reasonably conservative cut on the area (by eye) to avoid using the noisier data at the edges of the field.

All of the quasars have spectroscopic redshifts from their respective surveys, and optical photometry in the *ugriz* bands from the SDSS (York et al. 2000). We use these data to estimate the quasar luminosity, following Schneider et al. and others in using the absolute *i*-band magnitude, M_i, as a proxy for the luminosity of the central engine. This is calculated from the observed *i* magnitude (after the subtraction of Galactic extinction) and the redshift, by assuming a power-law SED ($S_\nu \propto \nu^\alpha$) with spectral index $\alpha = -0.5$ and assuming a Λ cold dark matter cosmology with $\Omega_m = 0.3$, $\Omega_\Lambda = 0.7$ and $H_0 = 70\,\mathrm{km\,s^{-1}\,Mpc^{-1}}$. Fig. 1 shows the distribution of optical luminosities of our sample as a function of redshift, indicating the source of the spectroscopic redshift (SDSS or 2SLAQ, or both). From this we can see that the 2SLAQ measurements in this field allow the inclusion of quasars at least 1 mag fainter (at $z < 3$) than the SDSS spectroscopic survey probes. This greater range in optical luminosity is crucial for decoupling optical luminosity and redshift, and gives our study an advantage over similar work by Hatziminaoglou et al. (2010). We note, however, that the range of bolometric luminosities spanned by our quasar sample is $10^{45} < L_{bol} < 10^{48}\,\mathrm{erg\,s^{-1}}$, so all of the objects are firmly in the quasar (as opposed to Seyfert) regime. Thus, if there are two 'modes' of accretion with different feedback properties, this study will only be relevant to understanding the 'quasar mode', making it usefully complementary to the work of Shao et al. (2010), which
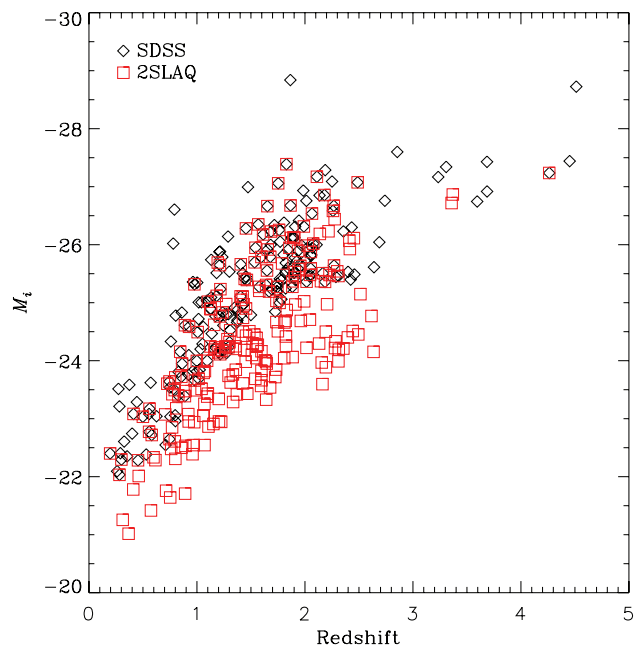
Figure 1. Absolute *i*-band magnitudes (calculated as described in the text) for our sample of spectroscopically confirmed quasars, plotted as a function of redshift. Objects with spectra from SDSS are shown as black diamonds; those with 2SLAQ spectra have red squares.

uses different *Herschel* data to probe the SFRs in lower luminosity X-ray-selected AGN.

Of the 372 quasars, only 29 have matches to objects in the 5σ H-ATLAS catalogue (Rigby et al. 2011; Smith et al. 2011). To improve our statistics, we measure fluxes directly from the SPIRE maps described by Pascale et al. (2011) at the position of each quasar. To do this, we take a point measurement of the flux in the nearest pixel to the SDSS position on each point-spread-function-filtered and background-subtracted map.

To account for source confusion, the most likely flux from the object (which is used to produce Fig. 2) is obtained by subtracting the mean pixel value in the map. However, when we perform a maximum-likelihood fit for the coefficients of equation (2), as described below, there is an implicit assumption that the measurement noise is symmetric about zero. The confusion noise is very significantly skewed, and can cause false correlations to be found in random data, so for the fluxes used in these fits we symmetrize the noise distribution by subtracting the flux in a different randomly selected pixel from each flux measurement. This increases the overall noise level, so we average the likelihoods from a number of random background realizations in order to reduce the noise level in the final result.

We also construct a comparison sample of fluxes drawn from random positions in the maps, with their backgrounds subtracted in precisely the same way as the real fluxes, and are then used to produce maximum-likelihood estimates in the same way as the real data. Comparing these estimates with those from the real data allows us to increase our confidence that any trend detected in the data is due to the influence of the quasars, and not merely a result of the noise properties of the maps, which have a significant impact due to our inclusion of individual noisy objects instead of using binned data.

To compare the AGN luminosity of the quasars with that from star formation, we make the assumption that the optical light is
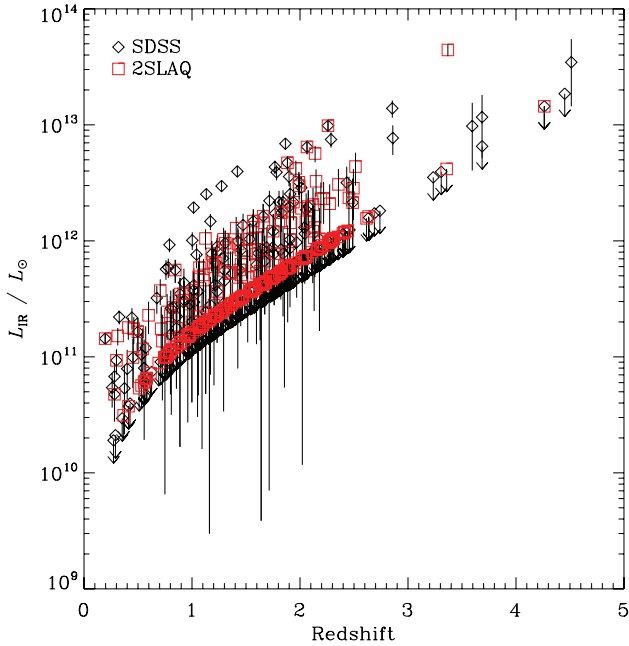
Figure 2. Estimated total infrared luminosities (calculated by integrating the best-fitting greybody with $T = 30$ K and $\beta = 1.5$ over the 8–1000 μm wavelength range) for our sample of spectroscopically confirmed quasars, plotted as a function of redshift. Objects with spectra from SDSS are shown as black diamonds; those with 2SLAQ spectra have red squares. Error bars are plotted where L_{IR} is greater than the uncertainty in the estimate, otherwise 1σ upper limits are shown using arrows.

dominated by the AGN, while the far-infrared/submm is dominated by the cool dust heated by star formation. This latter assumption is consistent with the results of Hatziminaoglou et al. (2010), who fit models with AGN and star formation contributions to the mid- and far-infrared emission from AGN hosts and find that star formation dominates the far-infrared fluxes. Their result depends on the assumption that the dusty torus heated directly by an AGN has a fairly simple, approximately toroidal geometry, as described by Fritz, Franceschini & Hatziminaoglou (2006). The infrared SEDs of AGN can, however, be fully reproduced by more complex clumpy torus models (e.g. Nenkova et al. 2008), so, at least until these models are tested by high spatial resolution imaging of AGN tori, we cannot completely rule out the possibility of a contribution to far-infrared fluxes from dust heated directly by the AGN. However, the fact that Hatziminaoglou et al. (2010) find that the SPIRE colours of AGN are indistinguishable from those of normal galaxies suggests that the AGN does not make a strong direct contribution at these wavelengths.

While the SPIRE photometry at 250, 350 and 500 μm is unlikely to be contaminated by the AGN directly for even the higher redshift quasars in the sample, this may not always be true for the shorter-wave length data from PACS. The H-ATLAS PACS photometry (Ibar et al. 2010) is also somewhat shallower, so we use only the SPIRE fluxes to constrain the overall infrared luminosity. To make the results directly comparable with each other, we fit a simple isothermal grey dust model, with flux density

$$S_\nu \propto \nu^{(3+\beta)}/(e^{h\nu/kT} - 1), \qquad (1)$$

where h and k are Planck's and Boltzmann's constants, ν is rest-frame frequency, and where we assume fixed values for both temperature $T = 30$ K and $\beta = 1.5$. We then integrate the greybody

curve between rest-frame wavelengths of 8 and 1000 μm to obtain an estimate of L_{IR}. (This wavelength range is chosen for convenience and for comparison with other studies, and is not intended to imply that the cold dust represented by the greybody dominates the SED at wavelengths as short as 8 μm.) We estimate the uncertainty on L_{IR} by increasing it until the χ^2 value for the fit to the data increases by unity.

Since we include far-infrared flux measurements at our quasar positions regardless of whether there is a significant detection in the far-infrared, fitting the normalization of a fixed template is the only robust measurement possible. This procedure does not account for the possibility of dust temperature or emissivity evolution either with redshift or quasar luminosity, which may well be important effects to consider. However, we are able to use the well-detected objects in our sample to address the suitability of our choice of T and β.

To check our choice of greybody temperature, we fit greybody SEDs to the SPIRE fluxes of individual quasars with good detections (signal-to-noise ratio > 3) in all the three SPIRE bands, with β fixed at 1.5 and T allowed to vary. The best-fitting temperatures for eight out of the nine well-detected quasars were very similar, with mean 32.4 K and a standard deviation of 2.8 K, while one outlier fits a temperature of $58.5^{+14.0}_{-7.5}$ K. The eight quasars span a redshift range of $1.1 < z < 2.3$ and a range in infrared luminosity (estimated by integrating the greybody between 8 and 1000 μm) of $6 \times 10^{12} < L_{IR}/L_\odot < 2 \times 10^{13}$. They are consistent with the temperatures of galaxies as a whole as determined by Amblard et al. (2010), who find a mean temperature of 28 ± 8 K for galaxies detected at a significance of 3σ in the H-ATLAS Science Demonstration Phase (SDP) field, and a mean temperature of 30 ± 9 K for a compilation of galaxies in H-ATLAS and a number of other far-infrared surveys. This consistency is unsurprising, since Elbaz et al. (2010) also found (using deeper data from *Herschel*) that the dust temperatures of radio-quiet AGN hosts were not significantly different from the normal galaxy population. Thus, we consider that a temperature $T = 30$ K is likely to be a reasonable choice for our quasar sample, but is not completely certain, and we return to this point later.

The outlying object has substantial uncertainties on its temperature, so we do not consider it an indication of a serious problem with our use of a single temperature for all objects. However, the fact that it is at a higher redshift ($z = 3.4$) and slightly higher luminosity ($L_{IR}/L_\odot = 3 \times 10^{13}$) than the other objects means that it is broadly consistent with the evolution of dust temperature, to higher temperatures at higher redshifts and luminosities, seen in several previous studies (Chapman et al. 2005; Kovács et al. 2006; Amblard et al. 2010; Michałowski, Hjorth & Watson 2010 and others).

We do not attempt to use a luminosity- or redshift-dependent dust temperature in this work. Increasing the dust temperature serves to shift the greybody peak to shorter wavelengths, which would result in a higher luminosity fit to our data (which are mostly longwards of the peak). Thus, if the temperature of the dust in quasar hosts does increase with redshift and/or luminosity, then we will systematically underestimate L_{IR} for objects at high redshift and L_{IR}. However, since the trend in mean temperature found by Amblard et al. is weak compared with the dispersion around the relation, we do not expect this to be a very significant effect.

To get an indication of the effect of temperature (and its uncertainty) on the parameters we derive, we perform fits to all objects using both $T = 30$ and 45 K, where we have selected 45 K because it has a similar peak wavelength to the average $z > 4$ quasar SED constructed by Priddey & McMahon (2001) (who find parameters of $T = 41 \pm 5$ K with $\beta = 1.95 \pm 0.3$). We also note that, while

β may not in fact be 1.5, the luminosity estimates obtained using $\beta = 2$ (using the best-fitting temperature at this β) differ by less than 1 per cent, so we consider that the selection of a value of β is broadly degenerate with the choice of T, at least for the purpose of estimating infrared luminosity from SPIRE fluxes.

Following SH09, we assume that the dependence of the infrared luminosity on the optical quasar luminosity and redshift can be expressed as power laws, i.e.

$$L_{\text{IR,model}} = A\, L_{\text{QSO}}^{\theta}\, (1 + z)^{\zeta}, \tag{2}$$

with intrinsic (Gaussian) dispersion in θ and ζ of $\Delta\theta$ and $\Delta\zeta$, respectively.

Unlike Serjeant & Hatziminaoglou, who stack infrared data to look for trends in bins of redshift and optical luminosity, we fit for the power-law coefficients of equation (2), and the normalization A, by finding the peak in the likelihood distribution calculated over all data simultaneously. Our approach has the substantial disadvantage that variations in the power laws as a function of redshift or luminosity will be hidden from us. However, under the assumption that the values of ζ and θ are the same at all redshifts and luminosities, our method enables us to make the most sensitive possible determination of these parameters, since we do not lose information through binning. Additionally, we are immune to the potentially confusing effects of correlations within bins.

We incorporate the dispersions $\Delta\theta$ and $\Delta\zeta$ by combining them with the uncertainty σ_i on each data point. The likelihood, Prob(data$|\theta, \zeta, \Delta\theta, \Delta\zeta, A$), at a given point in parameter space is then given by

$$\text{Prob}(\text{data}|\theta, \zeta, \Delta\theta, \Delta\zeta, A) = \prod_i \frac{e^{-\chi_i^2/2}}{\sqrt{2\pi\left(\sigma_i^2 + \sigma_{\theta,i}^2 + \sigma_{\zeta,i}^2\right)}}, \tag{3}$$

where

$$\chi_i^2 = \frac{(L_{\text{IR,data},i} - L_{\text{IR,model},i})^2}{\sigma_i^2 + \sigma_{\theta,i}^2 + \sigma_{\zeta,i}^2}, \tag{4}$$

$$\sigma_{\theta,i} = L_{\text{IR,model},i}\, \ln L_{\text{QSO},i}\, \Delta\theta \ \ \text{and} \tag{5}$$

$$\sigma_{\zeta,i} = L_{\text{IR,model},i}\, \ln(1 + z)\, \Delta\zeta\,. \tag{6}$$

The prior space on the parameters $\theta, \zeta, \Delta\theta, \Delta\zeta$ and A, over which the likelihood was evaluated, was chosen iteratively to enclose more than 99.999 per cent of the likelihood. The priors were linear in θ, ζ, $\Delta\theta$ and $\Delta\zeta$, and logarithmic in A, with the limits $\Delta\theta \geq 0$ and $\Delta\zeta \geq 0$.

4 RESULTS AND DISCUSSION

Fig. 3 shows the results of the likelihood evaluations, marginalized over all parameters except the two shown in each panel. This is the result of averaging the likelihoods obtained in 17 random realizations of the background, as described in Section 2. Contours labelled $1\sigma, 2\sigma, 3\sigma$ and 4σ enclose 68.3, 95.4, 99.73 and 99.994 per cent of the total likelihood. We show the results of fits assuming both $T = 30$ and 45 K to give an indication of the way in which our uncertainty in T should contribute to the uncertainty in the derived parameters.

This figure shows that, assuming the dust in quasars has a temperature $T = 30$ K, there is good evidence for correlations of L_{IR} with both L_{QSO} and z, since the maximum-likelihood values of both θ and ζ are significantly non-zero, and that while higher temperatures can mimic the effect of the correlation with z, the correlation with

L_{QSO} is robust to simple changes in the overall dust temperature. For the $T = 30$ K case, the best-fitting values of each parameter, with their 68.3 per cent confidence limits (marginalizing over all other parameters in each case), are

$$\theta = 0.22 \pm 0.08, \tag{7}$$

$$\zeta = 1.6 \pm 0.4, \tag{8}$$

$$\Delta\theta = 0.08 \pm\, ^{0.48}_{0.08} \tag{9}$$

and

$$\Delta\zeta = 3.4 \pm\, ^{0.9}_{0.7}. \tag{10}$$

Although, as can be seen in the lower left-hand panel of Fig. 3, there is some degeneracy between θ and ζ, our data exclude $\theta = 0$ at approximately the 2.5σ level. The (flat) prior on θ allowed it to take values between -1.5 and 1 (i.e. a much larger range than we show in Fig. 3), so we are confident that this is not simply an artefact of reaching the edge of the prior range.

The other panels of Fig. 3 show that there is not a strong degeneracy between any other parameters, so it is not possible to reproduce the effect of a correlation of L_{IR} with either L_{QSO} or z by simply increasing the intrinsic dispersion in the other parameter; indeed, these panels suggest that approximately the same result would be obtained if dispersion in the power-law indices was ignored altogether.

While the figure shows that the detected evolution of L_{IR} with redshift is very strongly dependent on the assumed value of T (although a temperature as high as 45 K for the whole sample seems unlikely), the correlation with L_{QSO} seems to be robust to this uncertainty. We find a slightly weaker index, θ, for the correlation with L_{QSO} than found by SH09, whose average result ($\theta = 0.44 \pm 0.07$) is shown in Fig. 3 as the point with error bars. This may in part be due to the relatively large redshift bins (e.g. $0.5 < z < 1$, $1 < z < 2$) which were used in SH09, since, because of the strong degeneracy between θ and ζ, these could allow trends with redshift to affect objects within a single bin. However, the disagreement is not very significant.

In contrast, performing the same maximum-likelihood fit to data with far-infrared fluxes drawn from random positions in the maps (with the same position used at each wavelength, and the dust-fitting performed assuming a temperature of 30 K), we obtain the results shown in Fig. 4. The important thing to note is that the best-fitting value of θ is zero for the random flux case, indicating that the result we have obtained is not simply due to the noise properties of the far-infrared maps, but rather is due to far-infrared flux genuinely associated with the quasars. (Note that the non-zero value for ζ derived from the fit to random data is not unexpected, since the real quasar luminosities and redshifts were still used in this case, and these are themselves correlated.)

Using deeper far-infrared data from *Herschel*, but with a narrower range in optical luminosity (because only SDSS, and not 2SLAQ, quasars are available in the field), Hatziminaoglou et al. (2010) find a very similar result, $\theta = 0.35$, for objects at redshifts $z > 2$. Serjeant et al. (2010) use a compilation of H-ATLAS and other data to find a weakly declining correlation between L_{IR} and quasar luminosity, parametrized as $\theta = (0.5875 \pm 0.045) - (0.09275 \pm 0.012)\,z$ for redshifts $0 < z < 4$, which is a slightly higher value of θ than we find, but broadly consistent within the errors and at the redshifts we are sensitive to. Our value of θ is also consistent with the work by Silverman et al. (2009), who find $\theta = 0.28 \pm 0.22$ for the slope of the power law relating [O II] luminosity (tracing star
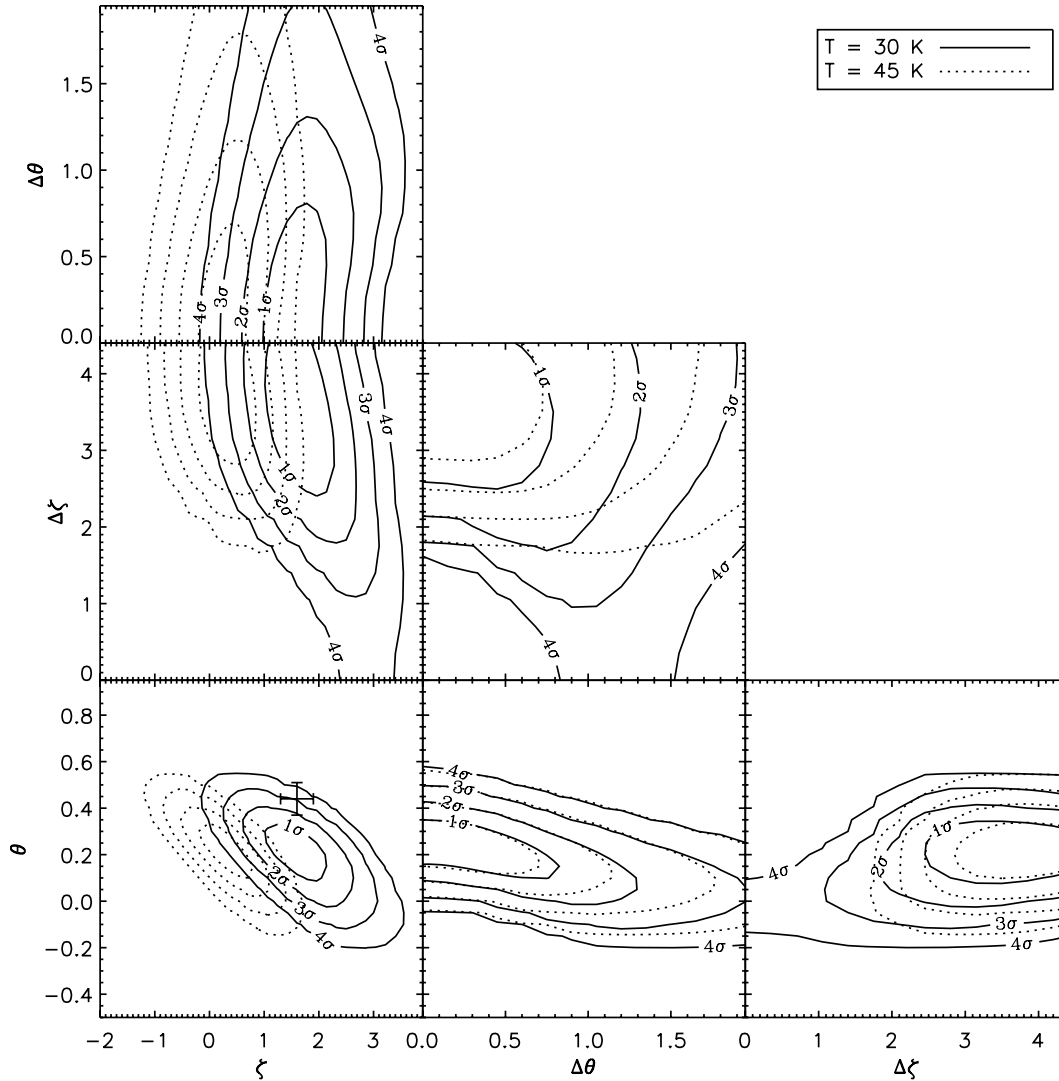
Figure 3. Likelihood contours for pairs of the parameters θ and ζ (from equation 2) and their intrinsic dispersions $\Delta\theta$ and $\Delta\zeta$, marginalized over the parameters not displayed in each panel. Contours labelled 1σ, 2σ, 3σ and 4σ enclose 68.3, 95.4, 99.73 and 99.994 per cent of the total likelihood. The point with error bars in the lower left-hand panel shows the average values of θ and ζ, and their 1σ uncertainties, determined by SH09 via stacking in the mid-infrared. Solid contours show a fit to objects assuming $T = 30$ K; dotted contours show a fit to the objects assuming $T = 45$ K.

formation after correcting for AGN contamination) to X-ray luminosity (tracing the AGN). Silverman et al. study a sample of AGN over a narrower range of redshifts ($0.5 < z < 1$) and with somewhat lower luminosities than most of our sample ($10^{44.3}$ erg s$^{-1} \lesssim L_{bol} \lesssim 10^{45.8}$ erg s^{-1}, assuming a bolometric correction $L_{bol}/L_{2-10keV} \sim 30$); the consistency of their result with ours suggests that the relationship between L_{IR} and L_{QSO} may not vary with L_{QSO} as suggested by Lutz et al. (2010) and Shao et al. (2010). Their steeper power law, with a slope of 0.8, for luminous quasars is not directly comparable with our result as it does not separate out the independent effect of redshift on L_{IR}. However, we would also note that the quasar part of this relationship is based on samples presented by Netzer (2009, and earlier works), which ignore AGN without detections in the far-infrared or mm, so that the observed correlation may be partly due to far-infrared flux limits.

To investigate whether our fit could be affected by a redshift dependence in θ, we perform the maximum-likelihood fitting again, using objects in restricted redshift ranges where we have enough objects to make a robust measurement, and marginalize over all parameters except θ. The results of this are shown in Fig. 5; the derived values of θ are not significantly different from each other for redshifts $0.5 < z < 2.5$, although the small number of objects in the redshift bins means we cannot make a strong statement for or against evolution of θ as a function of redshift. However, the $0.5 < z < 1$ range shows a detection of non-zero θ at better than the 2σ level, which is complementary to the result of Hatziminaoglou et al. (2010). While we do not have enough data to detect any significant decline in θ as a function of redshift, the data points in Fig. 5 are consistent with the relation found by Serjeant et al. (2010), and with our smaller H-ATLAS-only data set we cannot rule out the existence of such a weak redshift dependence.

Since the far-infrared luminosity L_{IR} has been shown to be due to star formation (Hatziminaoglou et al. 2010), the physical interpretation of these results is that SFR is higher both as redshift increases and as quasar luminosity increases. As was also suggested by SH09, and as has been incorporated into the 'quasar-mode' feedback recipes of semi-analytic models (e.g. Croton et al. 2006), one of the simplest ways to interpret this is if both black hole accretion
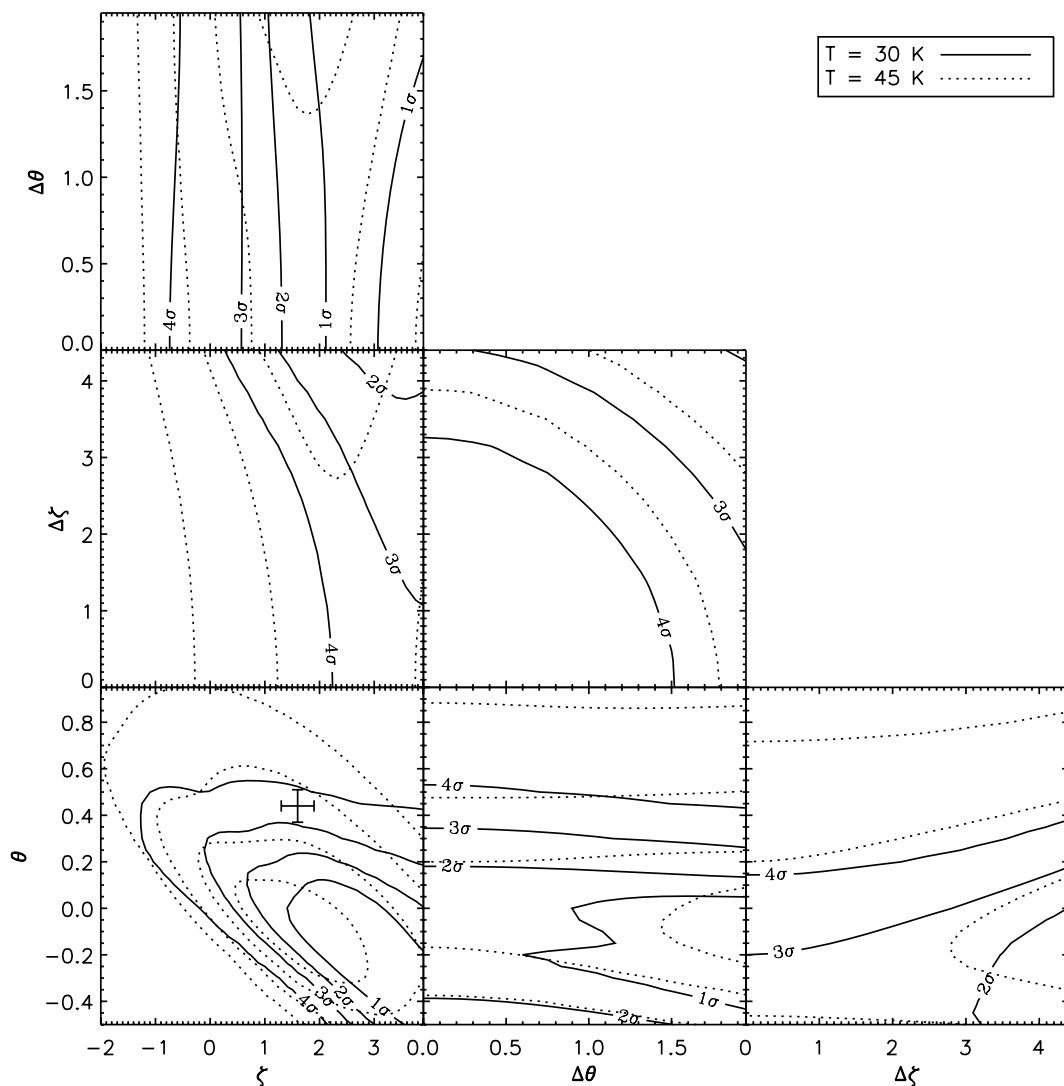
Figure 4. As Fig. 3 but with infrared fluxes drawn from random positions in the maps rather than from the quasar positions, as a check that the noise properties in the maps are not responsible for the correlation we detect between L_{IR} and L_{QSO}.

and star formation depend on a common supply of cold gas, as might be supplied during a galaxy–galaxy merger or cold-accretion event (Smith & Jarvis 2007; Smith et al. 2008; Dekel et al. 2009; Dijkstra & Loeb 2009). The implication of the non-unity slope is that the dependence of either star formation or accretion luminosity (or both) on the gas supply cannot simply be linear with gas mass, as one might naïvely suppose, but is instead more complex.

For both star formation and black hole accretion, such gas must be sufficiently cool that pressure support does not prevent it from being accreted by the AGN or from collapsing under its own gravity to form stars; so an alternative way to make this connection is via a mechanism (such as AGN or supernova feedback) which is capable of heating gas at all scales within a galaxy.

5 CONCLUSIONS

Using far-infrared measurements (at 250, 350 and 500 μm) of SDSS and 2SLAQ quasars in the H-ATLAS SD field, we find evidence for correlations between the infrared luminosities of quasar hosts with both redshift and quasar luminosity. While the best-fitting power-law index for the correlation with redshift can vary significantly

depending on the assumed temperature of the dust in the quasar hosts, the correlation with quasar luminosity is robust to this effect, and is non-zero at the 2.5σ level when we combine all objects in a maximum-likelihood fit.

We find a power-law index $\theta = 0.22 \pm 0.08$ for the relationship between L_{IR} and L_{QSO}. Our data show that θ is non-zero at the 2σ level in the $0.5 < z < 1$ redshift range alone, but we have too few objects to find evidence for evolution in θ over the range $0.5 < z < 2.5$.

We find evidence for a large intrinsic dispersion in the redshift dependence, but no evidence for intrinsic dispersion in the correlation between L_{QSO} and L_{IR}, suggesting that the latter is due to a direct physical connection between star formation and black hole accretion. One possible interpretation of this is that both the quasar activity and star formation are dependent on the same reservoir of cold gas, and are thus affected by influx of gas during mergers or cold accretion, or heating of gas via feedback processes.

With the full $550 \, \text{deg}^2$ of the H-ATLAS survey, we will be able to substantially increase the sample of quasars and improve these constraints. The larger area will allow us to obtain representative samples of the objects with the lowest density on the sky, i.e. quasars
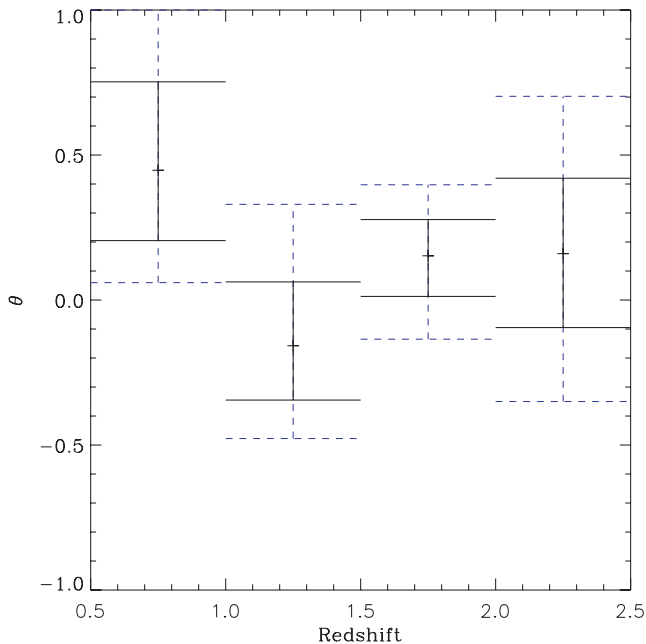
Figure 5. Best-fitting values of θ based on maximum-likelihood fits using data in the redshift ranges denoted by the widths of the error bars. Black, solid error bars are 68.3 per cent confidence limits; blue, dashed error bars are 95.4 per cent confidence limits.

with high luminosities at low redshift, which will increase the sensitivity of our test at low redshifts and permit us to remove the assumption of power-law correlations and test more general models. More importantly, a larger sample of objects at all redshifts will make it possible to measure the temperatures of dust in quasar hosts as a function of L_{QSO} and redshift by stacking the far-infrared fluxes; this in turn will remove the largest source of uncertainty in the relationship between L_{IR} and z.

REFERENCES

Alexander D. M., Bauer F. E., Chapman S. C., Smail I., Blain A. W., Brandt W. N., Ivison R. J., 2005, ApJ, 632, 736
Amblard A. et al., 2010, A&A, 518, L9
Antonucci R., 1993, ARA&A, 31, 473
Archibald E. N., Dunlop J. S., Hughes D. H., Rawlings S., Eales S. A., Ivison R. J., 2001, MNRAS, 323, 417
Bahcall J. N., Kirhakos S., Schneider D. P., 1994, ApJ, 435, L11
Baldi R. D., Capetti A., 2008, A&A, 489, 989
Benson A. J., Bower R. G., Frenk C. S., Lacey C. G., Baugh C. M., Cole S., 2003, ApJ, 599, 38
Bower R. G., Benson A. J., Malbon R., Helly J. C., Frenk C. S., Baugh C. M., Cole S., Lacey C. G., 2006, MNRAS, 370, 645
Chapman S. C., Blain A. W., Smail I., Ivison R. J., 2005, ApJ, 622, 772
Cole S., Lacey C. G., Baugh C. M., Frenk C. S., 2000, MNRAS, 319, 168
Croom S. M. et al., 2009, MNRAS, 392, 19
Croton D. J. et al., 2006, MNRAS, 365, 11
Dekel A. et al., 2009, Nat, 457, 451
Dijkstra M., Loeb A., 2009, MNRAS, 400, 1109
Dunlop J. S., McLure R. J., Kukula M. J., Baum S. A., O'Dea C. P., Hughes D. H., 2003, MNRAS, 340, 1095
Eales S. et al., 2010, PASP, 122, 499
Elbaz D. et al., 2010, A&A, 518, L29
Ferrarese L., Merritt D., 2000, ApJ, 539, L9
Fritz J., Franceschini A., Hatziminaoglou E., 2006, MNRAS, 366, 767
Gebhardt K. et al., 2000, ApJ, 539, L13
González-Nuevo J. et al., 2010, A&A, 518, L38
Granato G. L., Silva L., Monaco P., Panuzzo P., Salucci P., De Zotti G., Danese L., 2001, MNRAS, 324, 757
Granato G. L., De Zotti G., Silva L., Bressan A., Danese L., 2004, ApJ, 600, 580
Griffin M. J. et al., 2010, A&A, 518, L3
Guiderdoni B., Hivon E., Bouchet F. R., Maffei B., 1998, MNRAS, 295, 877
Hatziminaoglou E. et al., 2010, A&A, 518, L33
Herbert P. D., Jarvis M. J., Willott C. J., McLure R. J., Mitchell E., Rawlings S., Hill G. J., Dunlop J. S., 2010, MNRAS, 406, 1841
Ibar E. et al., 2010, MNRAS, 409, 38
Jahnke K., Macciò A., 2011, ApJ, 734, 92
Jarvis M. J. et al., 2001, MNRAS, 326, 1585
Kotilainen J. K., Falomo R., Decarli R., Treves A., Uslenghi M., Scarpa R., 2009, ApJ, 703, 1663
Kovács A., Chapman S. C., Dowell C. D., Blain A. W., Ivison R. J., Smail I., Phillips T. G., 2006, ApJ, 650, 592
Laird E. S., Nandra K., Pope A., Scott D., 2010, MNRAS, 401, 2763
Lutz D. et al., 2008, ApJ, 684, 853
Lutz D. et al., 2010, ApJ, 712, 1287
McLure R. J., Kukula M. J., Dunlop J. S., Baum S. A., O'Dea C. P., Hughes D. H., 1999, MNRAS, 308, 377
McLure R. J., Willott C. J., Jarvis M. J., Rawlings S., Hill G. J., Mitchell E., Dunlop J. S., Wold M., 2004, MNRAS, 351, 347
Magorrian J. et al., 1998, AJ, 115, 2285
Martínez-Sansigre A., Lacy M., Sajina A., Rawlings S., 2008, ApJ, 674, 676
Martínez-Sansigre A. et al., 2009, ApJ, 706, 184
Michałowski M., Hjorth J., Watson D., 2010, A&A, 514, A67
Nenkova M., Sirocky M. M., Nikutta R., Ivezić Ž., Elitzur M., 2008, ApJ, 685, 160
Netzer H., 2009, MNRAS, 399, 1907
Netzer H. et al., 2007, ApJ, 666, 806
Nolan L. A., Dunlop J. S., Kukula M. J., Hughes D. H., Boroson T., Jimenez R., 2001, MNRAS, 323, 308

Omont A., Beeler A., Bertoldi F., Cox P., Carilli C. L., Priddey R. S., McMahon R. G., Isaak K. G., 2003, A&A, 398, 857

Page M. J., Stevens J. A., Ivison R. J., Carrera F. J., 2004, ApJ, 611, L85

Pascale E. et al., 2011, MNRAS, 415, 911

Pilbratt G. L. A., 2010, A&A, 518, L1

Poglitsch A. et al., 2010, A&A, 518, L2

Priddey R. S., McMahon R. G., 2001, MNRAS, 324, L17

Priddey R. S., Isaak K. G., McMahon R. G., Robson E. I., Pearson C. P., 2003, MNRAS, 344, L74

Priddey R. S., Gallagher S. C., Isaak K. G., Sharp R. G., McMahon R. G., Butner H. M., 2007, MNRAS, 374, 867

Rigby E. et al., 2011, MNRAS, doi:10.1111/j.1365-2966.2011.19167.x

Sánchez S. F. et al., 2004, ApJ, 614, 586

Schneider D. P. et al., 2010, AJ, 139, 2360

Schweitzer M. et al., 2006, ApJ, 649, 79

Serjeant S., Hatziminaoglou E., 2009, MNRAS, 397, 265 (SH09)

Serjeant S. et al., 2010, A&A, 518, L7

Seymour N. et al., 2007, ApJS, 171, 353

Shao L. et al., 2010, A&A, 518, L26

Shi Y., Rieke G. H., Ogle P., Jiang L., Diamond-Stanic A. M., 2009, ApJ, 703, 1107

Silverman J. D. et al., 2009, ApJ, 696, 396

Smith D. J. B., Jarvis M. J., 2007, MNRAS, 378, L49

Smith D. J. B., Jarvis M. J., Lacy M., Martínez-Sansigre A., 2008, MNRAS, 389, 799

Smith D. et al., 2011, MNRAS, in press, preprint (arXiv:1007.5260)

Stevens J. A. et al., 2003, Nat, 425, 264

Stevens J. A., Jarvis M. J., Coppin K. E. K., Page M. J., Greve T. R., Carrera F. J., Ivison R. J., 2010, MNRAS, 405, 2623

Trichas M., Georgakak is A., Rowan-Robinson M., Nandra K., Clements D., Vaccari M., 2009, MNRAS, 399, 663

Trichas M. et al., 2010, MNRAS, 405, 2243

York D. G. et al., 2000, AJ, 120, 1579

This paper has been typeset from a TEX/LATEX file prepared by the author.